Supramolecular Chemistry
Publication details, including instructions for authors and subscription information:
http://www.informaworld.com/smpp/title~content=t713649759

Effect of hydrogen-bonded supramolecular assembling on liquid crystal properties of imidazole-containing azomethines and their chelates with copper(II)

Oleg N. Kadkin[a]; Jigeon Tae[a]; Eun Ho Kim[a]; So Yeon Kim[a]; Moon-Gun Choi[a]
[a] Department of Chemistry and Center for Bioactive Molecular Hybrids, BK21, Yonsei University, Seoul 120-749, Korea

First published on: 13 May 2009

To cite this Article Kadkin, Oleg N. , Tae, Jigeon , Kim, Eun Ho , Kim, So Yeon and Choi, Moon-Gun(2010) 'Effect of hydrogen-bonded supramolecular assembling on liquid crystal properties of imidazole-containing azomethines and their chelates with copper(II)', Supramolecular Chemistry, 22: 1, 1 — 12, First published on: 13 May 2009 (iFirst)
To link to this Article: DOI: 10.1080/10610270802709386
URL: http://dx.doi.org/10.1080/10610270802709386

Supramolecular Chemistry
Vol. 22, No. 1, January 2010, 1–12

Taylor & Francis
Taylor & Francis Group

Effect of hydrogen-bonded supramolecular assembling on liquid crystal properties of imidazole-containing azomethines and their chelates with copper(II)

Oleg N. Kadkin*, Jigeon Tae, Eun Ho Kim, So Yeon Kim and Moon-Gun Choi*

Department of Chemistry and Center for Bioactive Molecular Hybrids, BK21, Yonsei University, 262 Seongsanno, Seodaemun-Gu, Seoul 120-749, Korea

(*Received 24 September 2008; final version received 5 December 2008*)

A series of imidazole-containing rod-like Schiff's bases and their ionic copper(II) chelates with various lengths of the terminal alkyl chain containing 6, 8, 10, 12, 14 and 16 carbon atoms have been synthesised. The synthesised compounds were characterised by elemental analyses, ^{1}H NMR, IR and UV–vis and mass spectroscopies. Thermotropic smectic C mesophases in the ligands and smectic A mesophases in the copper(II) complexes were identified using POM, DSC and small-angle XRD scattering methods. X-ray diffraction patterns of the prepared imidazole imines indicate to supramolecular self-assembled structures in the liquid crystal state, which are formed by means of intermolecular hydrogen bonds. It was established that both liquid crystal arrangement and supramolecular assemblies in ligands disappeared near 190°C, mainly regardless of the lengths of the terminal alkyl chains. Contrary, assembling of the copper(II) complexes into supramolecular bilayers occurs near 200°C, which causes their transition to a smectic A mesophase.

Keywords: imidazole; liquid crystal; metallomesogen; Schiff's base; hydrogen bond; supramolecular assembling

Introduction

The heterocyclic systems of the class of imidazoles play a significant role as building blocks in biochemical systems such as alkaloids, histidine and histamine (*1*). Biological activity of imidazole derivatives is the main motive for their wide use in medicine, agriculture and pharmaceutical industry (*2*). Moreover, they also have a great potential in the area of optical and chemical sensors (*3*), fuel cell membranes (*4*), luminescent materials (*5*), ion-conducting electrolytes (*6*) and photovoltaic materials for solar cell applications (*7*). Even few of these instances are enough characterising imidazole as a fascinating chemical specie. As for known mesogenic imidazole derivatives, most of them belong to the class of ionic liquids, which are attracting increasing attention in many fields, including organic chemistry, electrochemistry and catalysis (*8*). Molecular imidazoles with mesogenic behaviour are less investigated, with the exception of several works that are mostly connected with using the imidazole moiety for creating supramolecular assemblies (*9*). Amphoteric character of the imidazole ring normally causes association of molecular imidazole compounds into agglomerates through intermolecular hydrogen bonds. Thus, interrelation between supramolecular organisation and liquid crystal properties in mesogenic imidazoles is rather interesting aspect for investigation. Besides the above-mentioned remarkable objects, metallomesogen systems, which are interesting from the standpoint of their optical, electric and magnetic properties, and also the crafting of nanostructured materials, have been constructed using the ability of these types of heterocycles to coordinate transition metals (*10*). Herein, we are reporting some new examples of the neutral molecular compounds from the class of Schiff's bases containing the 1*H*-imidazole fragment. In addition, prospectives of imidazole derivatives for obtaining ionic metallomesogen systems on their basis will be shown through the examples of the copper(II) chelates.

Results and discussion

Syntheses and characterisation

Synthetic routes towards imidazole-containig Schiff's bases and their copper(II) complexes are illustrated in Scheme 1. Reduction in nitrocompounds **1** (*11*) was carried out by catalytic hydrogenation on Pd/C (10%). The used method is the most preferable over all others in view of the fact that resulting anilines **2** trends towards forming coffee-coloured oxidation products during isolation and recrystallisation procedures. Clean and facile reduction with hydrogen allows to avoid excessive procedural operations with the reaction products, and to isolate easily pure amines **2**. Condensation of the obtained anilines **2** with 4(5)-imidazolyl carbaldehyde afforded target Schiff's bases **3** with the number of carbon atoms in the terminal alkyl chain between 6 and 16. Combining ethanol solutions

*Corresponding authors. Email: onk@yonsei.ac.kr; choim@yonsei.ac.kr

ISSN 1061-0278 print/ISSN 1029-0478 online

DOI: 10.1080/10610270802709386
http://www.informaworld.com

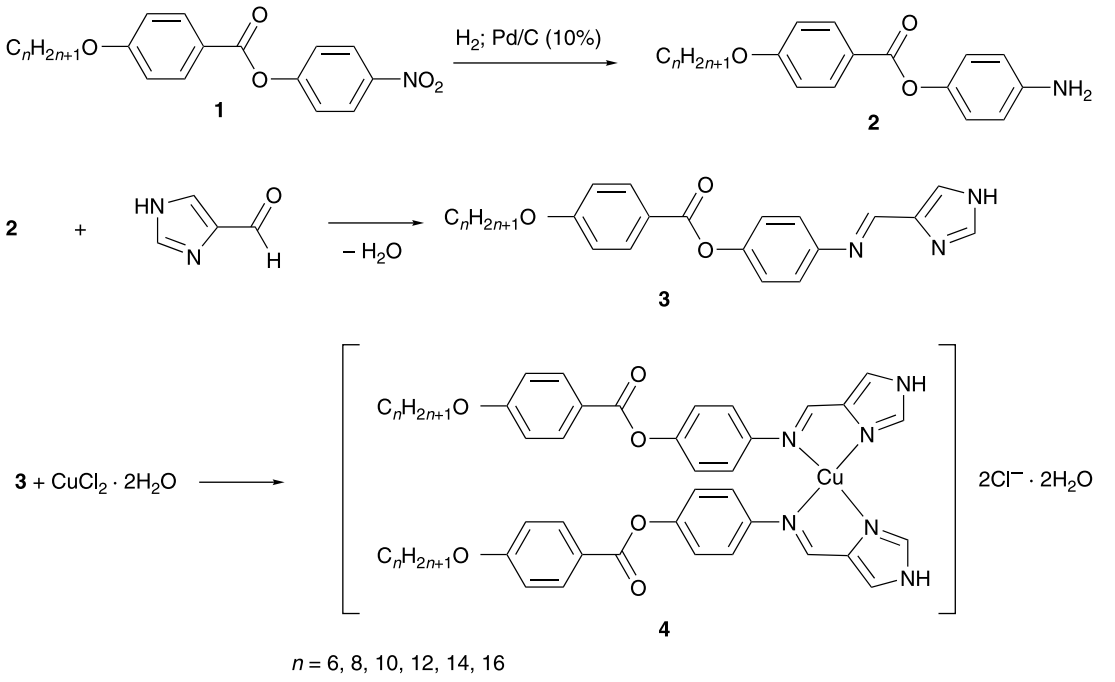

Scheme 1. Syntheses of the imidazole-containing Schiff's bases **3** and their copper(II) complexes **4**.

of the azomethines **3** and $CuCl_2{\cdot}2H_2O$ leads to precipitation of complexes **4**. It should be noted that N–H proton of an imidazole ring easily migrates between two nitrogen atoms, so there is always a tautomeric equilibrium existing between the two positional isomers.

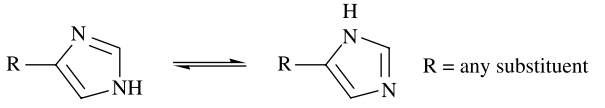

The synthesised anilines **2** gave satisfactory ^{1}H NMR spectra. Two vibration bands near 3450 and 3350 cm^{-1}, which are typically characterising secondary amines and associated with valence vibrations of the N–H bonds, were observed in the IR spectra of the series of **2**. Also, the valence stretching of the C═O bonds of the ester links can be straightforwardly identified at about 1720 cm^{-1}.

New imidazole-containing Schiff's bases **3** were unambiguously identified by the combination of elemental analyses, ^{1}H NMR, IR, UV–vis and mass spectroscopical methods. Proton signals of the imidazole ring and azomethine group are present in the ^{1}H NMR spectra of **3** as singlets in the area of 7.5–8.5 ppm. Slight broadening of the signals of the imidazole fragment was observed, which allowed to allocate the azomethine proton at 7.77 ppm distinguishing it from the imidazole signals. Apparently, signal spreading in the imidazole ring is connected with a tautomeric equilibrium due to the high mobility of the N–H protons. FT-IR spectra of **3** display the characteristic valence vibrational bands of the C═O bonds near 1730 cm^{-1} and C═N bonds at 1630 cm^{-1}. UV–vis spectra of compounds **3** are represented by two intensive absorption bands with maxima at about 275 and 315 nm, respectively. The first band was assigned to the $\pi-\pi^*$ electronic transitions of the imidazole ring, which is red shifted due to the conjugation with the CH═N group. The second band is seemingly associated with the azomethine chromophore.

Elemental analyses of the complexes **4** indicate that they contain two molecules of water in the hydrate sphere. It seems that not only the copper(II) and chloride ions but also the imidazole group strongly holds water molecules. The C═N bond stretching vibrations of the ligand in **4** are shifted bathochromically by 20 cm^{-1} in comparison with the uncomplexed Schiff's bases **3**. Further changes in the positions of the IR absorption bands in the region of 1000–1300 cm^{-1} and the appearance of new metal–ligand vibration modes near 550 and 610 cm^{-1} were observed upon the complex formation. Electronic spectra of the complexes **4** consist of two strong absorption maxima at about 270 and 340 nm, and one intensive shoulder near 320 nm. It can be concluded that the $\pi-\pi^*$ electronic transitions in the ligands at 320 nm are supplemented with metal-to-ligand charge-transfer absorptions at 340 nm in a series of **4**. Weak absorptions near 450 and 620 nm in the complexes were assigned to d–d transitions in the copper(II) ions. The arrangement of the first and second coordination spheres and geometrical configuration of the copper(II) complexes **4** are disputable; however, we propose octahedral surrounding with the

Table 1. Types of phase transitions, temperatures and the corresponding enthalpies from DSC thermograms for compounds **3** and **4**.

n	Compound	Transition	*T* (°C)	ΔH (kJ mol^{-1})
6	**3**	$cryst_1-cryst_2$	115.5	1.2
		$cryst_2$–iso	195	44.4
		iso–SmC[a]	[122]	[−2.0]
8	**3**	$cryst_1-cryst_2$	151	3.2
		$cryst_2$–SmC	184	32.8
		SmC–iso	191	3.0
10	**3**	$cryst_1-cryst_2$	131.5	5.35
		$cryst_2$–SmC	175	17.9
		SmC–iso	189	5.6
12	**3**	$cryst_1-cryst_2$	65	3.9
		$cryst_2-cryst_3$	127	12.9
		$cryst_3$–SmC	173	20.4
		SmC–iso	196	7.8
14	**3**	$cryst_1-cryst_2$	72	3.6
		$cryst_2-cryst_3$	130	15.8
		$cryst_3$–SmC	170	17.4
		SmC–iso	196	8.6
16	**3**	$cryst_1-cryst_2$	131	20.0
		$cryst_2$–SmC	167	17.2
		SmC–iso	190	8.7
6	**4**	$cryst_1-cryst_2$	184	5.5
		$cryst_2-cryst_3$	200	33.6
		$cryst_3$–SmA[b]	205	20.8
8	**4**	$cryst_1-cryst_2$	295	34.0
		$cryst_2$–SmA	204	20.1
10	**4**	cryst–SmA	198	39.6
12	**4**	cryst–SmA	206	35.4
14	**4**	$cryst_1-cryst_2$	75	7.1
		$cryst_2-cryst_3$	133	31.8
		$cryst_3-cryst_4$	172	35.3
		$cryst_4$–SmA	199	16.5
16	**4**	$cryst_1-cryst_2$	101	9.6
		$cryst_2-cryst_3$	138	6.3
		$cryst_3-cryst_4$	142	1.1
		$cryst_4-cryst_5$	157	4.1
		$cryst_5$–SmA	204	26.4

[a] Monotropic phase transition detected by POM at 160°C.
[b] The liquid crystal-to-isotropic liquid transitions for **4** were not detected as they lie higher than 290°C according to POM.

imidazole ligands in the equatorial edges and two chlorine ions in the two opposite vertexes. The last suggestion and some other structural features of the synthesised compounds will be interpreted lower in a close connection with their liquid crystallinity, XRD scattering data and supramolecular organisation by means of intermolecular hydrogen bonds.

Liquid crystal properties and supramolecular organisation

Thermal behaviour of both series of the ligands **3** and complexes **4** were investigated by a thermal polarisation optical microscopy (POM) and differential scanning calorimetry (DSC). In addition, several compounds, i.e. **3** ($n = 12, 14$) and **4** ($n = 12, 14$), were studied using the small-angle X-ray diffraction method at various temperatures. Data of the POM and DSC examinations are given in Table 1.

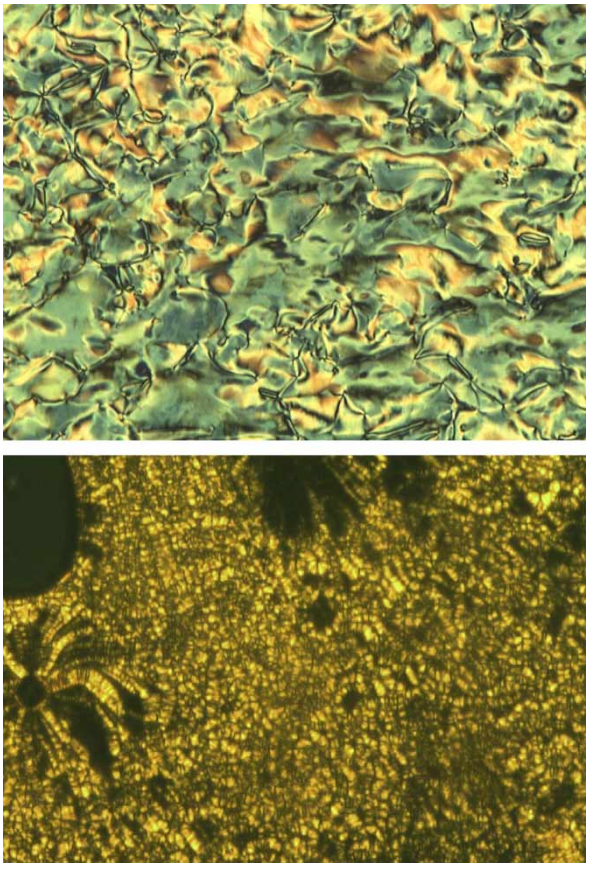

Figure 1. Optical textures observed under a polarisation microscope: a marbled schlieren texture of smectic C of **3** ($n = 14$) (upper microphotograph, on cooling from the isotropic liquid state at 185°C, 20×), and a polygonal texture of smectic A in **4** ($n = 12$) (lower microphotograph, on heating at 210°C, 50×).

All compounds in the series **3** exhibited enantiotropic smectic C mesophases with the exception of **3** ($n = 6$), which displayed monotropic smectic C mesomorphism. The compounds **3** have strong tendency towards vitrification upon cooling from the isotropic liquid state; hence, thermodynamics of the phase transitions on the second heating cycles was not investigated. Characterisitic POM textures observed in **3** on cooling from an isotropic liquid state are shown in Figure 1. A representative marbled schlieren texture given in the microphotograph is observed in all the compounds **3**, hence identifying a smectic C mesophase. The enthalpy values of liquid crystal-to-isotropic liquid transitions, which lie in a range between 3.0 and 9.0 kJ mol^{-1} depending on the length of the terminal alkyl chain, are also in a good agreement with this mesophase assignment.

Table 2. Crystal structure data of **3** and **4** obtained from XRD powder measurements at 25°C.

Compound	XRD peak intensity (a.u.)	Plains, Miller index	*d*-Spacing (Å)	Cell parameters				Molecular model dimensions[a]		
				a (Å)	*b* (Å)	*c* (Å)	*α* (°)	Length (Å)	Width (Å)	Thickness (Å)
3 ($n = 12$)	0.03	100	31.8	31.8	5.94	4.72	126.8	32.5	5.0	3.5
	0.11	010	4.76							
	0.13	011	4.59							
	0.02	111	4.36							
	0.02	001	3.78							
	0.02	101	3.52							
3 ($n = 14$)	0.18	100	34.8	34.8	5.89	4.71	126.6	34.9	5.0	3.5
	0.06	010	4.73							
	0.12	011	4.57							
	0.05	110	4.00							
	0.08	001	3.78							
	0.02	101	3.21							
4 ($n = 12$)	0.40	A[b]	66.0	34.5	12.45	6.84	115.2	34.8	9.5	6.0
	0.35	100	34.5							
	< 0.01	200	17.2							
	< 0.01	010	11.3							
	0.02	001	6.19							
	0.02	011	4.67							
	0.02	0 (−1)1	3.64							
4 ($n = 14$)	0.67	A	71.2	37.4	12.36	6.83	114.0	37.3	9.5	6.0
	0.10	100	37.4							
	< 0.01	200	18.7							
	< 0.01	010	11.3							
	0.07	001	6.24							
	0.07	011	4.69							
	0.07	111	4.23							
	0.07	0 (−1)1	3.64							

[a] Molecular modelling was performed using a standard computer program Hyperchem-7.1 (Hypercube, Inc., Gainesville, Florida, USA); a size of the minimal box suited to a single molecule is given.
[b] Compound **4** at 25°C is mainly a bilayered solid partially containing monolayered microcrystalline inclusions.

Besides, additional peaks assigned to crystal-to-crystal polymorphic transitions appeared in the DSC curves of **3**. The magnitudes of some DSC peaks of this type are not typical to a crystal-to-crystal phase transition (Table 1). Rather large enthalpy values indicate that they are associated with more intense transformations in the crystal structure. The latter statement is supported by XRD measurements as it will be discussed in lower paragraphs.

A polygonal texture of smectic A is detected in all the complexes **4** (Figure 1). Only crystal-to-smectic A phase transition is given for **4** as their isotropisation points were not observable because of thermal degradation of the samples after heating over 270–290°C. A birefringent texture of **4** remains at least up to these temperatures indicating a continued existence of the smectic A mesophase. Complexes **4** do not crystallise upon cooling from a smectic A mesophase preserving the liquid crystal arrangement in a solid glass state at room temperature. That was evidently distinguished by all POM, DSC and XRD investigations.

Generally, the melting points in a series of **3**, or otherwise transition temperatures from a crystal-to-liquid crystal phase, are decreased with the lengthening of the terminal alkyl chain. Such behaviour is typical for a homologous series of liquid crystals in a temperature region higher than 100°C. But it is rather unusual and intriguing that the comparatively same level of the clearing points were observed for all members of the series **3**. The same kind of close proximity of the phase transition temperatures, but in this case for a crystal-to-liquid crystal transitions, was also observed in a series of the copper(II) complexes **4**. In order to explain this phenomenon, we assumed a close relationship between the supramolecular organisation of **3** and **4** involving intermolecular hydrogen bonds and their liquid crystal properties.

In case of **3**, disengaging of hydrogen bonds occur roughly at the same temperatures, so parallel phase transformations in this connection do not depend on the lengths of the terminal alkyl chains. The ionic compound **4** has even more numerous possibilities for the supramolecular association not only connected with hydrogen bonds but also supplemented by ionic electrostatic interactions and coordination bonds. Supramolecular assembling in this case plays the same important role in liquid crystal ordering as traditional anisotropic interactions. Therefore, the formation of smectic layers in **4** involves primarily the

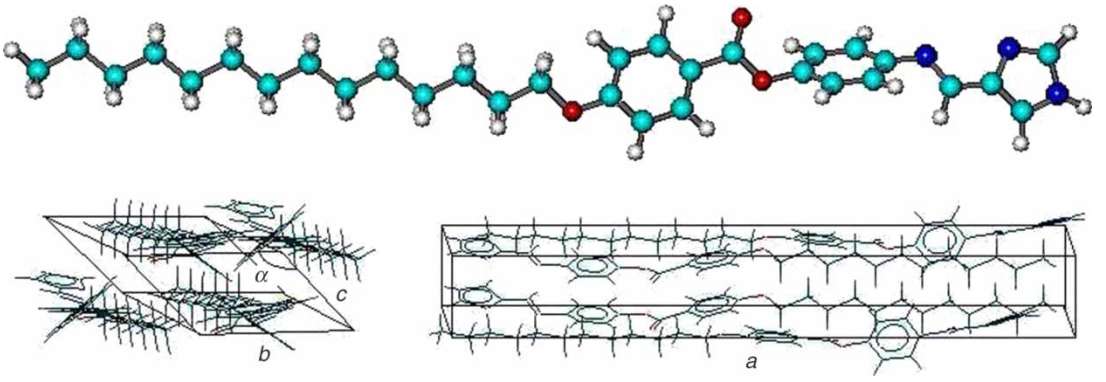

Figure 2. Molecular model and crystal packing of **3** ($n = 14$).

above-mentioned intermolecular interactions, and less depends on alterations in the anisotropy of polarisability for different lengths of the terminal alkyl chain. As a consequence, the mesophase transition temperatures remain almost the same for all members of a homologous series of **4**. Small-angle XRD scattering data at different temperatures allow to expose in some extent what kind of structural changes may occur during the phase transitions of **3** and **4**.

A monoclinic crystal system of the *P2/m* space group with the cell parameters represented in Table 2 was determined from the analysis of XRD scattering data of **3** ($n = 12$ and 14). The specified cell dimensions are in very good agreement with the corresponding computed models of a single molecule of **3** (Figure 2). We suppose that basically head-to-tail orientation of molecules by their elongated axes is realised in the long-range translational order of **3** at room temperature. This hypothesis is

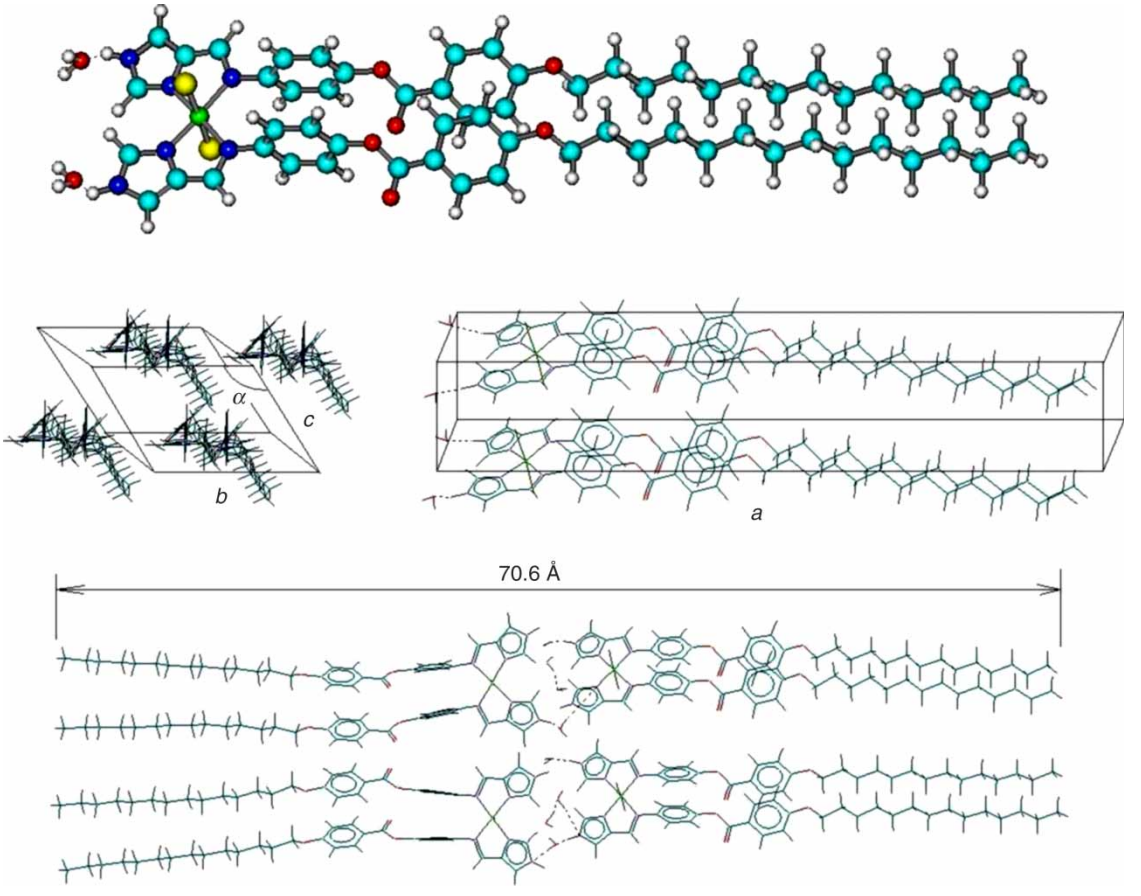

Figure 3. Molecular model and crystal packing of **4** ($n = 14$) and packing in bilayers.

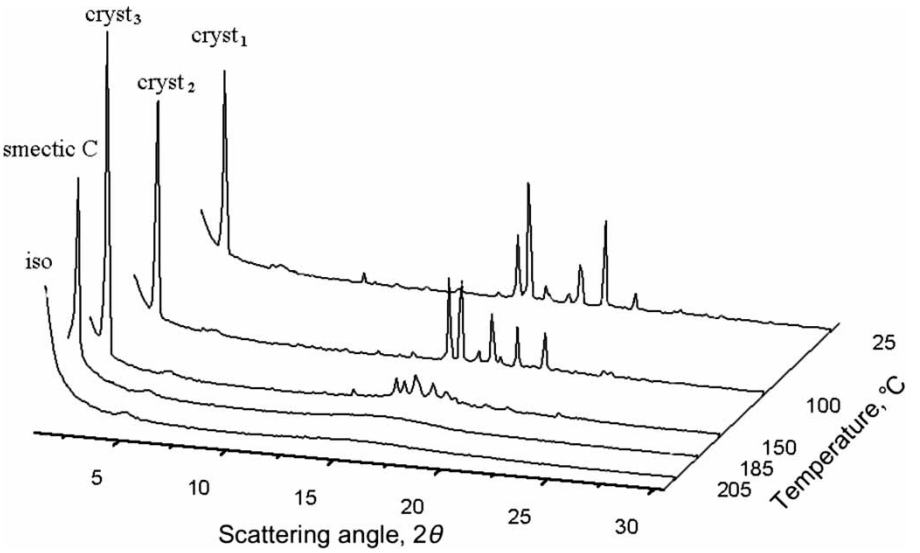

Figure 4. Development of crystal polymorphic modifications, smectic C and isotropic liquid phases of **3** ($n = 14$) on heating.

supported indirectly by the absence of the bilayers with the XRD peak corresponding to two-fold molecular length.

Molecular models of the complex **4** were built up presuming an octahedral coordination of copper(II) ion with the *cis*-orientation of the azomethine ligands and chlorine atoms positioned in two opposite vertexes. Plane-to-plane interactions of aromatic rings seem to be favourable for the proposed *cis*-alignment of ligands. Two hydrate molecules are placed instantly to the hydrophilic imidazole rings. A unit cell of the crystals of **4** conforms perfectly to this model by length in case of head-to-tail molecular orientation (Figure 3). The corresponding peak with a *d*-spacing equal to one molecular length is revealed in the XRD patterns of **4** (Table 2). But there is another more intensive XRD peak in a small-angle region with the layer distance almost twice exceeding the length of a molecule of **4**. An appropriate computed model of the bilayered structure illustrated in Figure 3 is rigorously matching by size to an interlayer distance found from the X-ray diffraction. Low intensity of XRD peaks in a medium angle region expose the absence of the strong long translational order within the bilayers. Thus, by all appearances, the copper(II) complexes **4** at room temperature mainly consist of bilayered solid with the close to amorphous structure and some monolayered crystalline matter.

Table 3. Variation in interlayer spacing upon phase transitions in **3** and **4**.

Compound	Temperature (°C)	Phase state	Interlayer spacing (Å)
3 ($n = 12$)	25	$crystal_1$	32.5
	100	$crystal_2$	33.2
	150	$crystal_3$	37.4
	185	smectic C	49.9
3 ($n = 14$)	25	$crystal_1$	34.8
	100	$crystal_2$	35.6
	150	$crystal_3$	39.3
	185	smectic C	51.6
4 ($n = 12$)	25	crystal	66.0[a]
	220	smectic A	55.4
4 ($n = 14$)	25	$crystal_1$	71.2
	90	$crystal_2$	71.2
	150	$crystal_3$	71.2
	175	$crystal_4$	68.0
	205	smectic A	59.8

[a] Space distance in the bilayered structure.

Subsequent metamorphoses in the XRD patterns of **3** ($n = 14$) during thermal phase transitions are illustrated in Figure 4. A peak in a small-angle region associated with the packing into layers with large periodicity appears in all crystal modifications and smectic C mesophase. No XRD peaks were observed in an isotropic liquid state. A group of XRD peaks in the area of *d*-spacings connected with positional ordering in the layers is presented only in crystal phases and transforms to a diffuse broad reflection in a smectic C mesophase. A significant decrease in intensity and sharpness of these peaks in a crystal state, which is preceding to a mesophase indicates to significant changes in the arrangement of the cell units, and is well correlated with the DSC data.

Profound changes in a *d*-spacing of the long periodicity were observed in **3** during evolution from a crystal-to-liquid crystal phase (Table 3). Positively, a huge increase in the interlayer distance in a smectic C mesophase in comparison with the prior values for a crystal state can be explained by segregation of amphiphilic molecules of **3** and the formation of bilayer

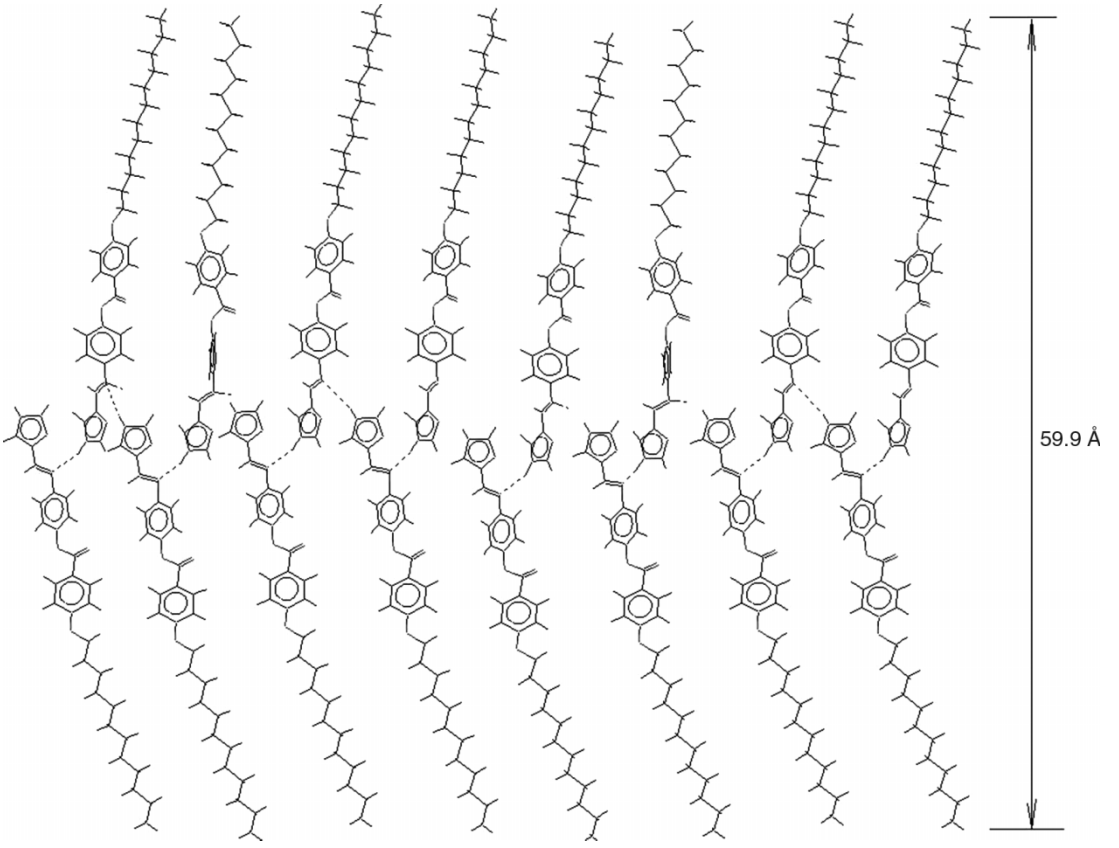

Figure 5. A computer model of the hydrogen-bonded supramolecular assembling in **3** ($n = 12$).

structures. Hydrogen-bonded chains provide additional stability to this kind of smectic bilayers (Figure 5). A calculated width of the supramolecular chains of **3** (60 Å for $n = 12$ and 65 Å for $n = 14$) exceeds an experimental *d*-spacing of the smectic layer (Table 3) that indicates to tilted structure of the latter by an angle 50–55°. Hence, the XRD data confirm additionally a smectic C mesophase assigned earlier by the POM and DSC investigations.

A solid state of the complexes **4** has more amorphous character than in the ligands **3**. As it was postulated before,

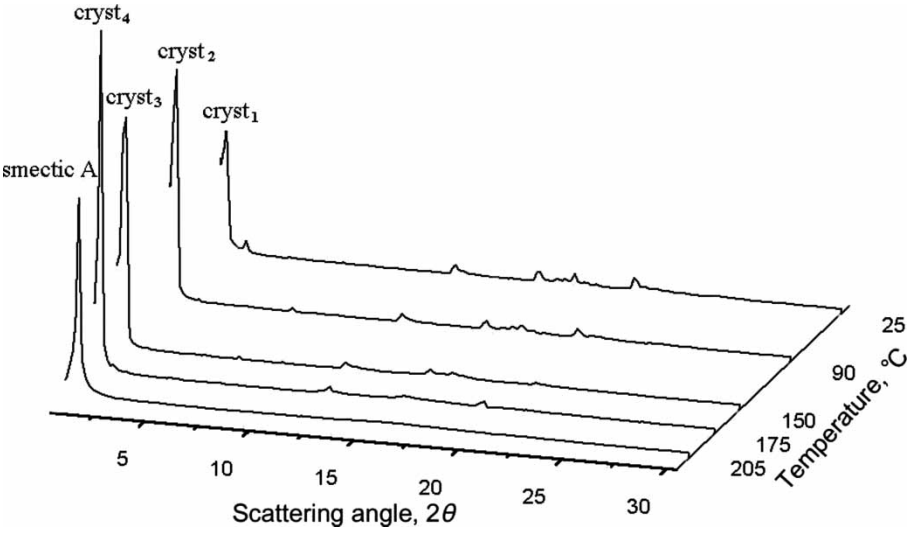

Figure 6. Development of crystal polymorphic modifications and smectic A mesophase of **4** ($n = 14$) on heating.

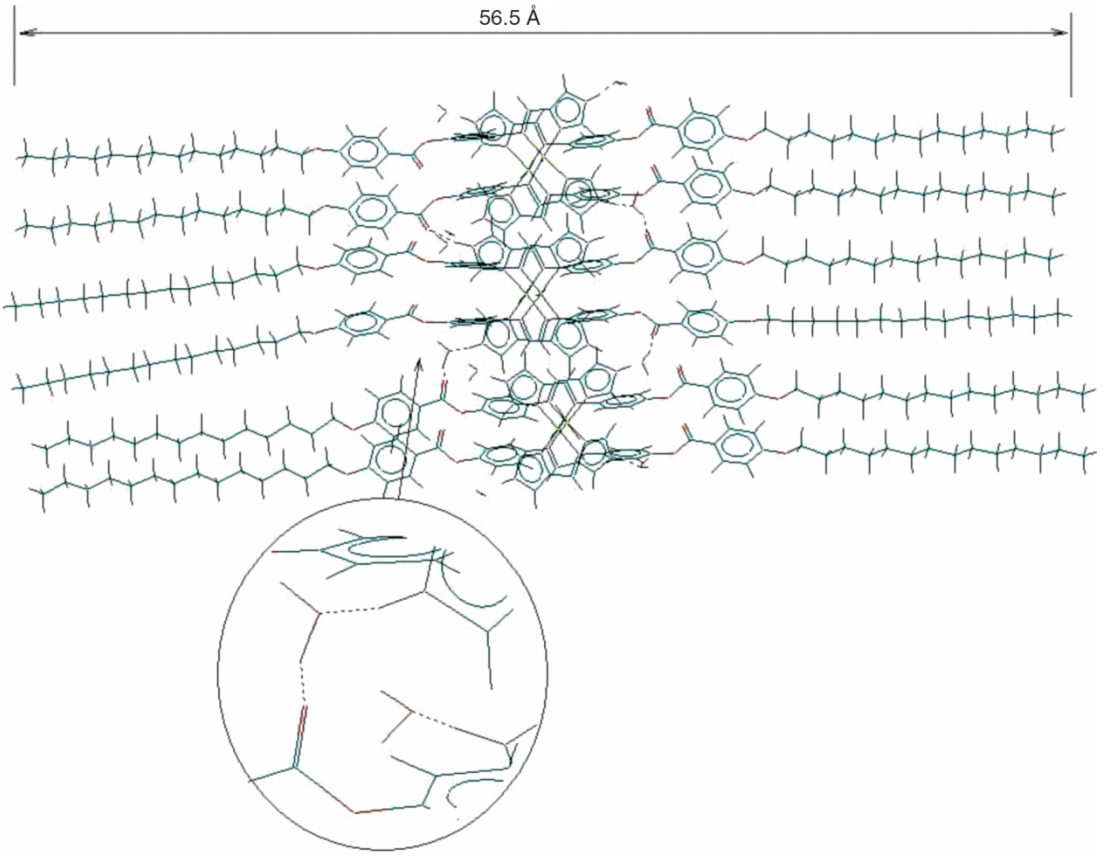

Figure 7. Interpenetrated double layer structure of **4** ($n = 14$).

there are bilayered structures present in **4** with head-to-head orientation of molecules. Gradual changes in XRD patterns during thermal development of a smectic A mesophase are shown in Figure 6. Small signals in a medium-angle region disappear completely in a smectic A state, but a small-angle peak associated with layers remains there. The most drastic changes occur in this time in the *d*-spacings of bilayers upon transition to a smectic mesophase (Table 3). A considerable decrease in the interlayer distance cannot be explained in a case of smectic A mesophase by a tilted structure of the layers. Only considering interpenetrating double layers, the calculated distance becomes close to the experimental *d*-spacing (Figure 7). A number of possibilities for electrostatic ionic and coordination interactions beside hydrogen bonds increase the stability of the interdigitated bilayered superstructure of **4** over 200°C contrary to hydrogen-bonded associates of **3**. Apparently, complexes **4** in a liquid crystal state can be classified to a certain extent as metallopolymer networks taking into account the exceptional thermal stability of the observed smectic A mesophases exceeding 290°C. Besides, a re-coordination of the copper(II) ions with the nitrogen donors from neighbouring molecules must be considered at the temperatures higher than 200°C, which facilitates cross-linking of the complexes **4**.

Experimental part

General details

Reagent grade chemicals and solvents were purchased from Aldrich (Yongin, Kyounggi-Do, Korea, Korea Branch), TCI (Tokyo, Japan) and Fluka (Yongin, Kyounggi-Do, Korea, Korea Branch). Solvents were dried and freshly distilled just before use. Melting points were determined by capillary method in a Stuart Scientific apparatus SMP3. Büchi Rotavapor R-124 was used to evaporate solvents from the reaction mixtures. The ^{1}H NMR spectra were measured on a Bruker AM 400 with TMS as internal standard. FT-IR spectra were performed on Nicolet Abatar-360 FT-IR spectrometer. UV–vis spectra in the region of 200–800 nm were recorded on a spectrophotometer Shimadzu UV-1650PC. Elemental analyses were performed on a Fisons instrument 2A1108 at Korea Institute of Science and Technology. DSC thermographs were obtained on PerkinElmer Diamond DSC with a scan rate of 10°C/min. Thermo-optical observations were carried out on a Nikon Eclipse E600 POL optical polarised

microscope equipped with a Mettler Toledo FP82 HT hot-stage system and Mettler FP90 central processor. Microphotographs were obtained with a Moticam 2300 digital camera. The X-ray scattering measurements were performed in transmission mode with synchrotron radiation of 1.3051 Å ($E = 9.5$ keV) at the 3C2 X-ray beamline at the Pohang Accelerator Laboratory (Pohang, Kyoungsangnam-Do, Korea). The sample was held in an aluminium sample holder, which was sealed with the window of 7-μm thick Kapton films in both sides. The sample was heated with two cartridge heaters and the temperature of the samples was monitored by thermocouple placed close to the sample.

Syntheses

4-Alkyloxybenzoic acids were prepared by applying standard Williamson procedure on ethyl-4-hydroxybenzoate and subsequent hydrolysis of the obtained alkoxylated esters as reported elsewhere (*11c, e*). 4-Nitrophenyl alkyloxybenzoates were synthesised by the *N,N′*-dicyclohexylcarbodiimide-assisted esterification of the corresponding benzoic acids with 4-nitrophenol (*11*).

*4-Aminophenyl-4-hexyloxybenzoate (**2**,* n = *6)*

4-Nitrophenyl-4′-hexyloxybenzoate (1.00 g, 2.91 mmol) was dissolved in a mixture of benzene–methanol (1:1, 80 ml). Then Pd/C (10%, wet, 0.40 g) was added to an obtained clear solution. The reaction proceeded in a hydrogenation apparatus under 2.5 atm pressure of hydrogen for 4 h. The resulted mixture was filtered through a layer of Celite 545 and evaporated in a vacuum rotary evaporator. Further purification by recrystallisation generally is not necessary as this may lead to obtaining brownish products. Yield: 0.89 g, 98%. White powder; mp 88–90°C; δ_H (250 MHz; $CDCl_3$; Me_4Si) 0.92 (t, $J = 7.5$ Hz, 3H, CH_3), 1.20–1.50 (m, 6H, CH_2), 1.82 (quintet, $J = 7.5$ Hz, 2H, OCH_2CH_2), 3.65 (br s, 2H, NH_2), 4.04 (t, $J = 6.5$ Hz, 2H, OCH_2), 6.97 (d, $J = 10.0$ Hz, 2H, aromatic), 7.05–7.25 (m, 4H, aromatic) and 8.12 (d, $J = 10.0$ Hz, 2H, aromatic); ν_{max} (KBr, cm^{-1}) 3440, 3370, 2920, 2849, 1715, 1605, 1513, 1277, 1256, 1192, 1166 and 1086.

*4-Aminophenyl-4-octyloxybenzoate (**2**,* n = *8)*

The compound was synthesised in a manner similar to 4-aminophenyl-4′-hexyloxybenzoate. Yield: 0.90 g, 98%. White powder; mp 137–140°C; δ_H (250 MHz; $CDCl_3$; Me_4Si) 1.07 (t, $J = 7.5$ Hz, 3H, CH_3), 1.20–1.50 (m, 10H, CH_2), 1.84 (quintet, $J = 7.5$ Hz, 2H, OCH_2CH_2), 3.65 (br s, 2H, NH_2), 4.01 (t, $J = 5.5$ Hz, 2H, OCH_2), 6.97 (d, $J = 10.0$ Hz, 2H, aromatic), 7.05–7.25 (m, 4H, aromatic) and 8.12 (d, $J = 10.0$ Hz, 2H, aromatic); ν_{max} (KBr, cm^{-1}) 3442, 3367, 2955, 2928, 2851, 2849, 1728, 1606, 1512, 1471, 1319, 1255, 1198, 1170, 1085 and 1014.

*4-Aminophenyl-4-decyloxybenzoate (**2**,* n = *10)*

The compound was synthesised in a manner similar to 4-aminophenyl-4′-hexyloxybenzoate. Yield: 1.41 g, 95%. White powder; mp 95–96°C; δ_H (250 MHz; $CDCl_3$; Me_4Si) 0.88 (t, $J = 7.5$ Hz, 3H, CH_3), 1.20–1.50 (m, 14H, CH_2), 1.79 (quintet, $J = 7.5$ Hz, 2H, OCH_2CH_2), 3.65 (br s, 2H, NH_2), 4.04 (t, $J = 5.5$ Hz, 2H, OCH_2), 6.97 (d, $J = 10.0$ Hz, 2H, aromatic), 7.05–7.20 (m, 4H, aromatic) and 8.12 (d, $J = 10.0$ Hz, 2H, aromatic); ν_{max} (KBr, cm^{-1}) 3435, 3371, 2953, 2920, 2863, 2851, 1724, 1606, 1513, 1472, 1316, 1279, 1259, 1200, 1167, 1082 and 1014.

*4-Aminophenyl-4-dodecyloxybenzoate (**2**,* n = *12)*

The compound was synthesised in a manner similar to 4-aminophenyl-4′-hexyloxybenzoate. Yield: 1.46 g, 98%. White powder; mp 99–101°C; δ_H (250 MHz; $CDCl_3$; Me_4Si) 0.88 (t, $J = 7.5$ Hz, 3H, CH_3), 1.20–1.50 (m, 18H, CH_2), 1.82 (q, $J = 7.5$ Hz, 2H, OCH_2CH_2), 3.65 (br s, 2H, NH_2), 4.04 (t, $J = 5.5$ Hz, 2H, OCH_2,), 6.97 (d, $J = 10.0$ Hz, 2H, aromatic), 6.90–7.00 (m, 4H, aromatic) and 8.12 (d, $J = 10.0$ Hz, 2H, aromatic); ν_{max} (KBr, cm^{-1}) 3459, 3372, 2918, 2849, 1715, 1605, 1513, 1277, 1256, 1192, 1166 and 1086.

*4-Aminophenyl-4′-tetradecyloxybenzoate (**2**,* n = *14)*

The compound was synthesised in a manner similar to 4-aminophenyl-4′-hexyloxybenzoate. Yield: 1.48 g, 99%. White powder; mp 98–101°C; δ_H (250 MHz; $CDCl_3$; Me_4Si) 0.88 (t, $J = 7.5$ Hz, 3H, CH_3), 1.20–1.50 (m, 22H, CH_2), 1.82 (q, $J = 7.5$ Hz, 2H, OCH_2CH_2), 3.65 (br s, 2H, NH_2), 4.04 (t, $J = 5.5$ Hz, 2H, OCH_2,), 6.97 (d, $J = 10.0$ Hz, 2H, aromatic), 7.05–7.20 (m, 4H, aromatic) and 8.12 (d, $J = 10.0$ Hz, 2H, aromatic); ν_{max} (KBr, cm^{-1}) 3455, 3347, 2917, 2849, 1728, 1606, 1512, 1255, 1203, 1171 and 1085.

*4-Aminophenyl-4′-hexadecyloxybenzoate (**2**,* n = *16)*

The compound was synthesised in a manner similar to 4-aminophenyl-4′-hexyloxybenzoate. Yield: 1.30 g, 95%. White powder; mp 100–102°C; δ_H (250 MHz; $CDCl_3$; Me_4Si) 0.88 (t, $J = 7.5$ Hz, 3H, CH_3), 1.20–1.50 (m, 26H, CH_2), 1.82 (q, $J = 7.5$ Hz, 2H, OCH_2CH_2), 3.65 (br s, 2H, NH_2), 4.04 (t, $J = 6.0$ Hz, 2H, OCH_2), 6.97 (d, $J = 10.0$ Hz, 2H, aromatic), 7.05–7.20 (m, 4H, aromatic) and 8.12 (d, $J = 10.0$ Hz, 2H, aromatic); ν_{max} (KBr, cm^{-1}) 3447, 3356, 2918, 2849, 1719, 1605, 1517, 1281, 1259, 1201, 1165 and 1083.

*4(5)-[4′-(4″-Hexyloxybenzoyloxy)phenyliminomethyl]-1H-imidazole (**3**,* n = *6)*

4-Aminophenyl-4′-(hexyloxy)benzoate (1.00 g, 3.19 mmol) and 4(5)-imidazole-carboxaldehyde (0.31 g, 3.19 mmol) were dissolved in hot ethanol separately. Two solutions were combined and refluxed for 30 min in the presence of 1–2 drops of acetic acid. A white precipitate was formed upon cooling. The product was filtered off and recrystallised from ethanol. Yield: 0.62 g, 50% (Found: C, 70.6; H, 6.4; N, 10.7; M^+, 391; $C_{23}H_{25}N_3O_3$: C, 70.6; H, 6.4; N, 10.7%; M, 391); ν_{max} (KBr, cm^{-1}) 2919, 2842, 1731, 1632, 1601, 1506, 1251, 1193, 1161 and 1065; λ_{max} (CH_2Cl_2, nm) 270 and 315 (log ε/dm^3 mol^{-1} cm^{-1} 4.03 and 3.82); δ_H (250 MHz; $CDCl_3$; Me_4Si) 0.92 (t, J = 7.5 Hz, 3H, CH_3), 1.20–1.50 (m, 6H, CH_2), 1.83 (quintet, J = 7.5 Hz, 2H, OCH_2CH_2), 4.05 (t, J = 5.5 Hz, 2H, OCH_2), 6.98 (d, J = 10.0 Hz, 2H, aromatic), 7.25 (d, J = 5.0 Hz, 4H, aromatic), 7.56 (s, 1H, imidazole), 7.77 (s, 1H, C*H*═N), 8.15 (d, J = 10.0 Hz, 2H, aromatic) and 8.40 (s, 1H, imidazole).

*4(5)-[4′-(4″-Octyloxybenzoyloxy)phenyliminomethyl]-1H-imidazole (**3**,* n = *8)*

The compound was prepared as described above for **3**, n = 6 starting from 4-aminophenyl-4′-(octyloxy)benzoate (1.00 g, 2.93 mmol) and 1H-imidazole-4(5)-carbaldehyde (0.28 g, 2.93 mmol). Yield: 0.61 g, 50% (Found: C, 71.7; H, 7.0; N, 10.0; M^+, 420; $C_{25}H_{29}N_3O_3$: C, 71.6; H, 7.0; N, 10.0%; M, 420); ν_{max} (KBr, cm^{-1}) 2920, 2846, 1732, 1631, 1603, 1504, 1252, 1197, 1160 and 1064; λ_{max} (CH_2Cl_2, nm) 275 and 316 (log ε/dm^3 mol^{-1} cm^{-1} 4.19 and 3.96); δ_H (250 MHz; $CDCl_3$; Me_4Si) 0.90 (t, J = 7.5 Hz, 3H, CH_3), 1.20–1.50 (m, 10H, CH_2), 1.83 (quintet, J = 7.5 Hz, 2H, OCH_2CH_2), 4.05 (t, J = 5.5 Hz, 2H, OCH_2), 6.98 (d, J = 10.0 Hz, 2H, aromatic), 7.25 (d, J = 5.0 Hz, 4H, aromatic), 7.57 (s, 1H, imidazole), 7.75 (s, 1H, C*H* = N), 8.15 (d, J = 10.0 Hz, 2H, aromatic) and 8.42 (s, 1H, imidazole).

*4(5)-[4′-(4″-Decyloxybenzoyloxy)phenyliminomethyl]-1H-imidazole (**3**,* n = *10)*

The compound was prepared as described above for **3**, n = 6 starting from 4-aminophenyl-4′-(decyloxy)benzoate (1.00 g, 2.71 mmol) and 1H-imidazole-4(5)-carbaldehyde (0.26 g, 2.71 mmol). Yield: 0.62 g, 52% (Found: C, 72.4; H, 7.5; N, 9.4; M^+, 448; $C_{27}H_{33}N_3O_3$: C, 72.45; H, 7.4; N, 9.4%; M, 448); ν_{max} (KBr, cm^{-1}) 2923, 2850, 1733, 1630, 1605, 1503, 1251, 1198, 1162 and 1064; λ_{max} (CH_2Cl_2, nm) 274 and 316 (log ε/dm^3 mol^{-1} cm^{-1} 4.30 and 4.08); δ_H (250 MHz; $CDCl_3$; Me_4Si) 0.89 (t, J = 7.5 Hz, 3H, CH_3), 1.20–1.50 (m, 14H, CH_2), 1.83 (quintet, J = 7.5 Hz, 2H, OCH_2CH_2), 4.05 (t, J = 5.5 Hz, 2H, OCH_2), 6.98 (d, J = 10.0 Hz, 2H, aromatic), 7.25 (d, J = 5.0 Hz, 4H, aromatic), 7.58 (s, 1H, imidazole), 7.77 (s, 1H, C*H*═N), 8.15 (d, J = 10.0 Hz, 2H, aromatic) and 8.42 (s, 1H, imidazole).

*4(5)-[4′-(4″-Dodecyloxybenzoyloxy)phenyliminomethyl]-1H-imidazole (**3**,* n = *12)*

The compound was prepared as described above for **3**, n = 6 starting from 4-aminophenyl-4′-(dodecyloxy)-benzoate (1.00 g, 2.52 mmol) and 1H-imidazole-4(5)-carbaldehyde (0.24 g, 2.52 mmol). Yield: 0.80 g, 67% (Found: C, 73.0; H, 7.9; N, 8.8; M^+, 476; $C_{29}H_{37}N_3O_3$: C, 73.2; H, 7.8; N, 8.8%; M, 476); ν_{max} (KBr, cm^{-1}) 2920, 2851, 1731, 1629, 1603, 1505, 1250, 1198, 1161 and 1063; λ_{max} (CH_2Cl_2, nm) 277 and 316 (log ε/dm^3 mol^{-1} cm^{-1} 4.49 and 3.83); δ_H (250 MHz; $CDCl_3$; Me_4Si) 0.88 (t, J = 7.5 Hz, 3H, CH_3), 1.20–1.50 (m, 18H, CH_2), 1.82 (quintet, J = 7.5 Hz, 2H, OCH_2CH_2), 4.04 (t, J = 5.5 Hz, 2H, OCH_2), 6.98 (d, J = 10.0 Hz, 2H, aromatic), 7.25 (d, J = 5.0 Hz, 4H, aromatic), 7.57 (s, 1H, imidazole), 7.77 (s, 1H, C*H*═N), 8.14 (d, J = 10.0 Hz, 2H, aromatic) and 8.42 (s, 1H, imidazole).

*4(5)-[4′-(4″-Tetradecyloxybenzoyloxy)phenyliminomethyl]-1H-imidazole (**3**,* n = *14)*

The compound was prepared as described above for **3**, n = 6 starting from 4-aminophenyl-4′-(tetradecyloxy)-benzoate (1.00 g, 2.35 mmol) and 1H-imidazole-4-carbaldehyde (0.23 g, 2.35 mmol). Yield: 0.84 g, 75% (Found: C, 73.85; H, 8.3; N, 8.35; M^+, 504; $C_{31}H_{41}N_3O_3$: C, 73.9; H, 8.2; N, 8.3%; M, 504); ν_{max} (KBr, cm^{-1}) 2923, 2845, 1731, 1632, 1602, 1506, 1251, 1201, 1161 and 1066; λ_{max} (CH_2Cl_2, nm) 275 and 316 (log ε/dm^3 mol^{-1} cm^{-1} 4.17 and 3.95); δ_H (250 MHz; $CDCl_3$; Me_4Si) 0.88 (t, J = 7.5 Hz, 3H, CH_3), 1.20–1.50 (m, 22H, CH_2), 1.83 (quintet, J = 7.5 Hz, 2H, OCH_2CH_2), 4.05 (t, J = 5.5 Hz, 2H, OCH_2), 6.98 (d, J = 10.0 Hz, 2H, aromatic), 7.25 (d, J = 5.0 Hz, 4H, aromatic), 7.58 (s, 1H, imidazole), 7.78 (s, 1H, C*H* = N), 8.15 (d, J = 10.0 Hz, 2H, aromatic) and 8.42 (s, 1H, imidazole).

*4(5)-[4′-(4″-Hexadecyloxybenzoyloxy)phenyliminomethyl]-1H-imidazole (**3**,* n = *16)*

The compound was prepared as described above for 4(5)-[4′-(4″-hexyloxybenzoyloxy)phenyliminomethyl]-1H-imidazole starting from 4-aminophenyl-4′-(hexadecyloxy)benzoate (1.00 g, 2.21 mmol) and 1H-imidazole-4-carbaldehyde (0.21 g, 2.21 mmol). Yield: 0.76 g, 65% (Found: C, 74.3; H, 8.6; N, 7.9; M^+, 532; $C_{33}H_{45}N_3O_3$: C, 74.5; H, 8.5; N, 7.9%; M, 532); ν_{max} (KBr, cm^{-1}) 2922, 2849, 1732, 1633, 1601, 1504, 1252, 1198, 1160 and 1065;

λ_{max} (CH_2Cl_2, nm) 273 and 316 (log ε/dm^3 mol^{-1} cm^{-1} 4.39 and 4.03); δ_H (250 MHz; $CDCl_3$; Me_4Si) 0.88 (t, $J = 7.5$ Hz, 3H, CH_3), 1.20–1.50 (m, 26H, CH_2), 1.82 (quintet, $J = 7.5$ Hz, 2H, OCH$_2$CH_2), 4.05 (t, $J = 5.5$ Hz, 2H, OCH_2), 6.98 (d, $J = 10.0$ Hz, 2H, aromatic), 7.25 (d, $J = 5.0$ Hz, 4H, aromatic), 7.58 (s, 1H, imidazole), 7.78 (s, 1H, CH = N), 8.15 (d, $J = 10.0$ Hz, 2H, aromatic) and 8.42 (s, 1H, imidazole).

*Bis-{4-[4′-(4″-hexyloxybenzoyloxy)phenyliminatomethyl]-1-imidazolato}copper(II) dichloride dihydrate (**4**, n = 6)*

Ligand **3**, $n = 6$ (100 mg, 0.26 mmol) and $CuCl_2 \cdot 2H_2O$ (23 mg, 0.13 mmol) were dissolved in hot ethanol separately. Two solutions were combined and the reaction mixture was stirred for 30 min at 60°C. A light greenish precipitate formed upon complexation, which was centrifugated, and then an ethanol layer was pipetted off from a centrifuge tube. The solid layer was washed with ethanol 2× using the same centrifugation method. Fine light greenish powder was dried for several days in a vacuumed desiccator with P_2O_5. Yield: 95 mg, 81% (Found: C, 57.7; H, 5.6; N, 9.0; $C_{46}H_{54}Cl_2CuN_6O_8$: C, 57.95; H, 5.7; N, 8.8%); ν_{max} (KBr, cm^{-1}) 2922, 2849, 1732, 1633, 1601, 1504, 1252, 1198, 1160 and 1065; λ_{max} (CH_2Cl_2, nm) 270 (log ε/dm^3 mol^{-1} cm^{-1} 4.12), 313 sh (3.65), 338 (3.92), 450 sh (3.70) and 600 sh (3.31).

*Bis-{4-[4′-(4″-octyloxybenzoyloxy)phenyliminatomethyl]-1-imidazolato}copper(II) dichloride dihydrate (**4**, n = 8)*

Prepared similarly as above from ligand **3**, $n = 8$ (100 mg, 0.24 mmol) and $CuCl_2 \cdot 2H_2O$ (21 mg, 0.12 mmol). Yield: 110 mg, 92% (Found: C, 60.4; H, 6.0; N, 8.4; $C_{50}H_{62}Cl_2CuN_6O_8$: C, 59.5; H, 6.2; N, 8.3%)[1]; ν_{max} (KBr, cm^{-1}) 2922, 2849, 1732, 1633, 1601, 1504, 1252, 1198, 1160 and 1065; λ_{max} (CH_2Cl_2, nm) 273 (log ε/dm^3 mol^{-1} cm^{-1} 4.18), 308 sh (3.75), 338 (3.82), 450 sh (3.61) and 600 sh (3.21).

*Bis-{4-[4′-(4″-decyloxybenzoyloxy)phenyliminatomethyl]-1-imidazolato}copper(II) dichloride dihydrate (**4**, n = 10)*

Prepared similarly as above from ligand **3**, $n = 10$ (100 mg, 0.22 mmol) and $CuCl_2 \cdot 2H_2O$ (19 mg, 0.11 mmol). Yield: 100 mg, 89% (Found: C, 60.5; H, 6.4; N, 7.9; $C_{54}H_{70}Cl_2CuN_6O_8$: C, 60.9; H, 6.6; N, 7.9%); ν_{max} (KBr, cm^{-1}) 2922, 2849, 1732, 1633, 1601, 1504, 1252, 1198, 1160 and 1065; λ_{max} (CH_2Cl_2, nm) 269 (log ε/dm^3 mol^{-1} cm^{-1} 4.24), 306 sh (4.08), 336 (4.08), 450 sh (3.66) and 600 sh (3.32).

*Bis-{4-[4′-(4″-dodecyloxybenzoyloxy)phenyliminatomethyl]-1-imidazolato}copper(II) dichloride dihydrate (**4**, n = 12)*

Prepared similarly as above from ligand **3**, $n = 12$ (100 mg, 0.21 mmol) and $CuCl_2 \cdot 2H_2O$ (18 mg, 0.11 mmol). Yield: 64 mg, 56% (Found: C, 61.1; H, 6.8; N, 7.5; $C_{58}H_{78}Cl_2CuN_6O_8$: C, 62.1; H, 7.0; N, 7.5%)[2]; ν_{max} (KBr, cm^{-1}) 2922, 2849, 1732, 1633, 1601, 1504, 1252, 1198, 1160 and 1065; λ_{max} (CH_2Cl_2, nm) 275 (log ε/dm^3 mol^{-1} cm^{-1} 4.31), 313 sh (4.15), 338 (4.05), 450 sh (3.47) and 600 sh (3.01).

*Bis-{4-[4′-(4″-tetradecyloxybenzoyloxy)phenyliminatomethyl]-1-imidazolato}copper(II) dichloride dihydrate (**4**, n = 14)*

Prepared similarly from ligand **3**, $n = 14$ (100 mg, 0.20 mmol) and $CuCl_2 \cdot 2H_2O$ (18 mg, 0.11 mmol). Yield: 110 mg, 98% (Found: C, 63.7; H, 7.3; N, 7.3; $C_{62}H_{86}Cl_2CuN_6O_8$: C, 63.2; H, 7.4; N, 7.1%); ν_{max} (KBr, cm^{-1}) 2922, 2849, 1732, 1633, 1601, 1504, 1252, 1198, 1160 and 1065; λ_{max} (CH_2Cl_2, nm) 261 (log ε/dm^3 mol^{-1} cm^{-1} 4.04), 307 sh (3.98), 333 (3.99), 450 sh (3.72) and 600 sh (3.25).

*Bis-{4-[4′-(4″-hexadecyloxybenzoyloxy)phenyliminatomethyl]-1-imidazolato}copper(II) dichloride dihydrate (**4**, n = 16)*

Prepared similarly from ligand **3**, $n = 16$ (100 mg, 0.19 mmol) and $CuCl_2 \cdot 2H_2O$ (16 mg, 0.09 mmol). Yield: 70 mg, 65% (Found: C, 64.1; H, 7.5; N, 6.9; $C_{66}H_{94}Cl_2CuN_6O_8$: C, 64.2; H, 7.7; N, 6.8%); ν_{max} (KBr, cm^{-1}) 2922, 2849, 1732, 1633, 1601, 1504, 1252, 1198, 1160 and 1065; λ_{max} (CH_2Cl_2, nm) 252 (log ε/dm^3 mol^{-1} cm^{-1} 4.14), 312 sh (4.06), 342 (4.06), 450 sh (3.71) and 600 sh (3.33).

Conclusions

A series of imidazole-containing rod-like Schiff's bases and their ionic copper(II) chelates displaying, respectively, smectic C and A mesophases have been synthesised. A variation in the length of the terminal alkyl chains within 6, 8, 10, 12, 14 and 16 carbon atoms does not influence significantly on the clearing points of the synthesised azomethines and melting points of their complexes. Such behaviour is justified herein assuming considerable regulation of these phase transitions by assembling and disassembling of supramolecular structures. The proposed molecular arrangement of smectic layers in both series of the compounds is founded on hydrogen bonds, and plus ionic and coordination interactions in a case of the copper(II) complexes. Related superstructures have been

investigated by the small-angle X-ray scattering method. There is a very good resemblance between the computer models of the proposed supramolecular assemblies and experimental *d*-spacings determined from the X-ray diffraction experiments.

Acknowledgements

This work has been supported by the programme Brain Korea 21 (BK-21) and the Centre for Bioactive Molecular Hybrids (KOSEP).

Notes

1. Element analyses given here and in the cases below were slightly deviated from the acceptable range. Insolubility of the Cu(II) complexes in common solvents does not allow to perform their recrystallisation, while in more polar solvents like DMF, the complexes seemed to be unstable.
2. See above.

References

(1) Brown, E.G. *Ring Nitrogen and Key Biomolecules*; Kluwer Academic Publishers: Dordrecht/Boston/London, 1998.

(2) Pozharskii, A.F.; Soldatenkov, A.T.; Katritzky, A.R. *Heterocycles in Life and Society*; John Wiley & Sons: Chichester, 1997.

(3) (a) Fukuda, N.; Kim, J.Y.; Fukuda, T.; Ushijima, H.; Tomada, K. *Jpn. J. Appl. Phys.* **2006**, *45*, 460–464. (b) Chao, H.; Ye, B.-H.; Zhang, Q.-L.; Ji, L.-N. *Inorg. Chem. Commun.* **1999**, *2*, 338–340.

(4) (a) Schuster, M.; Meyer, W.H.; Wegner, G.; Herz, H.G.; Ise, M.; Kreuer, K.D.; Maier, J. *Solid State Ionics* **2001**, *145*, 85–92. (b) Münch, W.; Kreuer, K.-D.; Silvestri, W.; Maier, J.; Seifert, G. *Solid State Ionics* **2001**, *145*, 437–443. (c) Pu, H.; Qiao, L. *Macromol. Chem. Phys*. **2005**, *206*, 263–267.

(5) (a) Knölker, H.-J.; Hitzemann, R.; Boese, R. *Chem. Ber.* **1990**, *123*, 327–339. (b) Zhao, L.; Li, S.B.; Wen, G.A.; Peng, B.; Huang, W. *Mater. Chem. Phys.* **2006**, *100*, 460–463.

(6) (a) Yoshio, M.; Kagata, T.; Hoshino, K.; Mukai, T.; Ohno, H.; Kato, T. *J. Am. Chem. Soc.* **2006**, *128*, 5570–5577. (b) Kishimoto, K.; Suzawa, T.; Yokota, T.; Mukai, T.; Ohno, H.; Kato, T. *J. Am. Chem. Soc*. **2005**, *127*, 15618–15623. (c) Yoshio, M.; Mukai, T.; Ohno, H.; Kato, T. *J. Am. Chem. Soc.* **2004**, *126*, 994–995.

(7) Wang, M.; Xiao, X.; Zhou, X.; Li, X.; Lin, Y. *Sol. Energy Mater. Sol. Cells* **2007**, *91*, 785–790.

(8) (a) Binnemans, K. *Chem. Rev.* **2005**, *105*, 4148–4204. (b) Bowlas, C.J.; Bruce, D.W.; Seddon, K.R. *Chem. Commun.* **1996**, 1625–1626. (c) Gordon, C.M.; Holbrey, J.D.; Kennedy, A.R.; Seddon, K.R. *J. Mater. Chem*. **1998**, *8*, 2627–2636. (d) Dobbs, W.; Douce, L.; Allouche, L.; Louati, A.; Malbose, F.; Welter, R. *New J. Chem.* **2006**, *30*, 528–532. (e) Chiou, J.Y.Z.; Chen, J.N.; Lei, J.S.; Lin, I.J.B. *J. Mater. Chem*. **2006**, *16*, 2972–2977. (f) Lee, K.-M.; Lee, Y.-T.; Lin I.J.B. *J. Mater. Chem*. **2003**, *13*, 1079–1084. (g) Kouwer, P.H.J.; Swager, T.M. *J. Am. Chem. Soc*. **2007**, *129*, 14042–14052. (h) Bradley, A.E.; Hardacre, C.; Holbrey, J.D.; Johnston, S.; McMath, S.E.J.; Nieuwenhuyzen, M. *Chem. Mater.* **2002**, *14*, 629–635. (i) Li, L.; Groenewold, J.; Picken, S.J. *Chem. Mater.* **2005**, *17*, 250–257.

(9) (a) Pisula, W.; Dierschke, F.; Müllen, K. *J. Mater. Chem.* **2006**, *16*, 4058–4064. (b) Osuji, C.O.; Chao, C.-Y.; Ober, C.K.; Thomas, E.L. *Macromolecules* **2006**, *39*, 3114–3117. (c) Seo, S.H.; Park, J.H.; Tew, G.N.; Chang, J.Y. *Tetrahedron Lett.* **2007**, *48*, 6839–6844. (d) Seo, S.H.; Tew, G.N.; Chang, J.Y. *Soft Mater.* **2006**, *2*, 886–891. (e) Cardinaels, T.; Ramaekers, J.; Nockemann, P.; Driesen, K.; Van Hecke, K.; Van Meervelt, L.; Lei, S.; De Feyter, S.; Guillon, D.; Donnio, B.; Binnemans, K. *Chem. Mater.* **2008**, *20*, 1278–1291.

(10) (a) Lee, C.K.; Ling, M.J.; Lin, I.J.B. *Dalton Trans.* **2003**, 4731–4737. (b) Hsu, S.J.; Hsu, K.M.; Leong, M.K.; Lin, I.J.B. *Dalton Trans*. **2008**, 1924–1931. (c) Lo, Y.-S.; Chen, W.-S.; Yang, J.-Y.; Lin, I.J.B.; Wu, M.-H.; Shih, M.-C. *Thin Solid Films* **2008**, *516*, 1175–1182; (d) Suisse, J.-M.; Douce, L.; Bellemin-Laponnaz, S.; Maisse-Francois, A.; Welter, R.; Miyake, Y.; Shimizu, Y. *Eur. J. Inorg. Chem.* **2007**, 3899–3905.

(11) (a) Soulivong, D.; Ziessel, R.; Matt, D.J. *Organomet. Chem.* **1994**, *474*, 207–215. (b) Morrone, S.; Guillon, D.; Bruce, D.W. *Inorg. Chem.* **1996**, *35*, 7041–7048. (c) Guillevic, M.-A.; Danks, M.J.; Harries, S.K.; Collinson, S.R.; Pidwell, A.D.; Bruce, D.W. *Polyhedron* **2000**, *19*, 249–257. (d) Lee, J.-W.; Jin, J.-I.; Achard, M.F.; Hardouin, F. *Liq. Cryst.* **2001**, *28*, 663–671. (e) Narasimhaswamy, T.; Somanathan, N.; Lee, D.K.; Ramamoorthy, A. *Chem. Mater.* **2005**, *17*, 2013–2018. (f) Majumdar, K.C.; Pal, N.; Nath, S.; Choudhury, S.; Rao, N.V.S. *Mol. Cryst. Liq. Cryst.* **2007**, *461*, 37–51.